Materials Science and Engineering B 177 (2012) 61–68

Contents lists available at SciVerse ScienceDirect

Materials Science and Engineering B

journal homepage: www.elsevier.com/locate/mseb

Diffusion barrier characteristics and shear fracture behaviors of eutectic PbSn solder/electroless Co(W,P) samples

Hung-Chun Pan, Tsung-Eong Hsieh *

Department of Materials Science and Engineering, National Chiao Tung University, 1001 Ta-Hsueh Road, Hsinchu 30010, Taiwan, ROC

A R T I C L E I N F O

Article history:
Received 12 May 2011
Received in revised form
13 September 2011
Accepted 26 September 2011
Available online 6 October 2011

Keywords:
Electroless Co(W,P)
IMC
Diffusion barrier
Shear test

A B S T R A C T

Diffusion barrier characteristics, activation energy (E_a) of IMC growth and bonding properties of amorphous and polycrystalline electroless Co(W,P) (termed as α-Co(W,P) and poly-Co(W,P)) to eutectic PbSn solder are presented. Intermetallic compound (IMC) spallation and an nano-crystalline P-rich layer were observed in PbSn/α-Co(W,P) samples subjected to liquid-state aging at 250 °C. In contrast, IMCs resided on the P-rich layer in PbSn/α-Co(W,P) samples subjected to solid-state aging at 150 °C. Thick IMCs neighboring to an amorphous W-rich layer was seen in PbSn/poly-Co(W,P) samples regardless of the aging type. α-Co(W,P) was found to be a sacrificial- plus stuffed-type barrier while poly-Co(W,P) is mainly a sacrificial-type barrier. The values of E_a's for PbSn/α-Co(W,P) and PbSn/poly-Co(W,P) systems were 338.6 and 167.5 kJ/mol, respectively. Shear test revealed the ductile mode dominates the failure in both α- and poly-Co(W,P) samples. Analytical results indicated the high P content in electroless layer might enhance the barrier capability but degrade the bonding strength.

© 2011 Elsevier B.V. All rights reserved.

1. Introduction

As an essential component of flip-chip (FC) bonding for advanced electronic packaging, the under bump metallurgy (UBM) is the multilayer thin-film structure comprised of adhesion, diffusion barrier and wetting/protection layers. The diffusion barrier layer inhibits the interdiffusion between bump body and bond pad materials so as to ensure the reliable operation of integrated circuits (ICs). Diffusion barrier can be classified as sacrificial type, stuffed type, passive-compound type and amorphous type according to the mechanisms to inhibit the interdiffusion [1]. Refractory metals such as tungsten (W), molybdenum (Mo), platinum (Pt), palladium (Pd) and rhodium (Rh) prepared by physical vapor deposition (PVD) have adopted as the barrier layer in conventional FC structures. It was also found that the thin layers prepared by “wet” process, *e.g.*, electroless nickel (EN), may also serve as the diffusion barrier layers for the advantages including high throughput, high step coverage, lower stress status, and free of grain boundary for short-circuit diffusion [2–6]. Electroless cobalt–phosphorus (Co(P)) possesses a superior barrier capability to inhibit the interdiffusion between Cu and the interlayer dielectric (ILD) in Cu-ICs [7] and it might also inhibit the diffusion of PbSn solder [8]. Kohn et al. reported the enhancement of thermal stability and diffusion barrier capability to Cu metallization by incorporating the W element in electroless Co(P) [9,10] and our study on amorphous electroless Co(W,P) revealed it may serve as a mixed type barrier, *i.e.*, a combination of sacrificial and stuffed type, to PbSn solder and Cu [11]. In this study, we prepare the amorphous and polycrystalline electroless Co(W,P) (termed as α-Co(W,P) and poly-Co(W,P) hereafter) layers and their diffusion barrier capabilities to eutectic PbSn solder are evaluated *via* the liquid- and solid-state aging tests. Scanning electron microscopy (SEM) and transmission electron microscopy (TEM) in conjunction with energy dispersive spectroscopy (EDS) were employed to analyze the microstructure evolution at PbSn/Co(W,P) interfaces. The experimental findings also provide the information regarding of the activation energies (E_a's) of IMC growth in the diffusion couples containing α-Co(W,P) or poly-Co(W,P) subjected to the solid-state aging. The solder ball shear test was also carried out to elucidate the bonding characteristics of various PbSn/Co(W,P) samples so as to clarify the practical applicability of electroless Co(W,P) layers to FC bonding. The fracture surfaces subjected to shear test were also examined by SEM in order to identify the corresponding fracture mode.

2. Experimental methods

Silicon (Si) wafers coated with Ti (50 nm)/Cu (100 nm) layer to simulate the adhesion layer and the Cu interconnects were adopted as the substrates of this study. Prior to the electroless plating, a pretreatment including roughening, sensitization and activation was performed in order to yield the Co(W,P) layers with better structure

* Corresponding author. Tel.: +886 3 5712121x55306, fax: +886 3 5724727.
E-mail address: tehsieh@mail.nctu.edu.tw (T.-E. Hsieh).

0921-5107/$ – see front matter © 2011 Elsevier B.V. All rights reserved.
doi:10.1016/j.mseb.2011.09.037

Table 1
Chemicals and processing conditions of pretreatment [11].

Step	Component	Concentration	Immersion time
Roughening	H_2SO_4	5 wt.%	30 s
Sensitization	$SnCl_2{\cdot}2H_2O$ HCl	10 g/L 40 ml/L	5 min
Activation	$PdCl_2{\cdot}2H_2O$ HCl	0.1 g/L 8 ml/L	1 min

integrity. Afterward, about 6- to 8-μm thick electroless Co(W,P) layer was deposited on the Cu/Ti/Si substrate. Tables 1 and 2 separately list the formulations and processing conditions for pretreatment and electroless plating process [11]. The pH value of plating bath was monitored by using a pH meter and adjusted with a 3 M KOH solution so as to achieve the Co(W,P) layers with desired crystallinities. The α-Co(W,P) and the poly-Co(W,P) were separately obtained at pH = 8.6 and 7.6. Subsequent compositional analysis indicated the P content is about 9.1–10.2 at.% and W content is about 0.4–0.9 at.% in α-Co(W,P) whereas the P content is about 4–6 at.% and the W content is about 5–8 at.% in poly-Co(W,P). Immediately after the Co(W,P) deposition, an appropriate amount of eutectic PbSn solder paste was applied on the Co(W,P) surface and a brief reflow at 250 °C for 30 s was performed in order to solidify the solder. The PbSn/electroless Co(W,P)/Cu/Ti/Si samples were annealed in N_2 atmosphere for liquid-state aging at 250 °C for up to 5 h or vacuum-sealed and sent to furnace for solid-state aging test at 150 °C for 1000 h. For the determination of the E_a's of IMC growth in various samples, solid-state aging at 130 and 170 °C for at least 500 h were also performed and, for the purpose of comparison, the PbSn/pure Co samples were prepared by applying the PbSn solder paste on pure Co foil and tested at the same conditions. SEM (Jeol JSM-6500F or Hitachi S-4700) and TEM (Philips Tecnai F-20) in conjunction with EDS (Genesis) were adopted to examine the microstructure and composition changes in the samples. The cross-sectional TEM (XTEM) samples were prepared by using the focused-ion-beam (FIB, FEI-201) technique supported by Materials Analysis Technology, Inc. at Chupei, Taiwan, ROC. At least four different locations were analyzed by EDS and the average results were presented as the composition data of samples. As to samples for ball shear test, an array of circular bond pad pattern with 200 μm in diameter was formed on the substrates deposited with α-Co(W,P) or poly-Co(W,P) by the photolithography process using an SU-8 permanent photoresist (supplier: MicroChem Corp.; 5%-weight-loss thermal decomposition temperature = 279 °C in air) as the mask layer. After attaching the 300-μm-diameter PbSn solder balls on the pads, a reflow treatment in N_2 atmosphere at 250 °C for 1, 10, 20, 30 and 60 min was then carried out to form the solder ball joints. The shear test was performed in accord with the JEDEC Standard, JESD22-B117A [12], by using a Dage 4000 multipurpose bond-tester supported by Schmidt Scientific Taiwan Ltd. at Hsinchu, Taiwan, ROC. The shear tool standoff = 30 μm above the sample surface and shear speed = 100 μm/s. The average shear force was deduced from the results of at least 25 bumps for each sample preparation condition.

Table 2
Chemicals and processing conditions of electroless Co(W,P) plating [11].

Component		Concentration (g/L)
Co source	$CoSO_4{\cdot}7H_2O$	23
Reducing agent	$NaH_2PO_2{\cdot}H_2O$	18
Complexing agent	Na_3 citrate	144
Buffer agent	H_3BO_3	31
W source	$Na_2WO_4{\cdot}2H_2O$	10
pH value		7.6 or 8.6
Temperature		90 °C

3. Results and discussion

3.1. PbSn/α-Co(W,P) samples

Fig. 1(a)–(f) presents the cross-sectional SEM micrographs of PbSn/α-Co(W,P) couples subjected to liquid-state aging for as-reflow, 20 min, 30 min, 1 h, 3 h and 5 h, respectively. We note the prolonged liquid-state aging is for examining a complete microstructure evolution in such a sample type. As shown in Fig. 1(a), granular $CoSn_2$ intermetallic compound (IMC) coated with $CoSn_3$ by the peritectic reaction [11] or $CoSn_3$ IMCs emerged at the solder/Co(W,P) interface at the early stage of aging. Voids were occasionally observed and they might be caused by the evaporation of organic additives in the solder paste. In the sample subjected to 20-min aging, the IMCs coarsen and detachment of IMCs away from the reacting interface occurs as shown in Fig. 1(b). In addition, an about 1-μm thick continuous layer neighboring to unreacted Co(W,P) can be observed and the EDS analysis reveals it contains about 20 at.% of P and about 2.3 at.% of W. As a result of the accumulation of P elements at the reacting interface, such a P-rich layer is in fact a mixture of nano-scale IMCs as reported by our previous study [11]. The spallation of IMCs became rather obvious after the aging for 30 min as shown in Fig. 1(c) and nearly all IMCs spalled into solder after 1-h aging as depicted by Fig. 1(d). The SEM images shown in Fig. 1(e) and (f) indicate that there is no dramatic change in interfacial morphology in the samples subjected to prolonged aging in which the thickness of P-rich layer remains the same at about 1 μm.

Above results seem to indicate that the formation of continuous P-rich layer may deter subsequent Co–Sn reactions. In order to verify this phenomenon, a 250 °C/30-min aged sample was further aged at 150 °C for 200 h. As shown in Fig. 2, the growth of secondary IMCs from the P-rich layer into solder was observed. A supply of Co and Sn elements would be required for forming such bush-like IMCs, implying the P-rich layer cannot block the Co–Sn interdiffusion and the IMC spallation is in fact an unceasing process at the reacting interface during liquid-state aging. This also indicates the P accumulation at the reacting interface plays a key role in the evolution of interfacial morphology. When the P content at reacting interface remains low at the early stage of aging, the IMCs form and reside at the solder/Co(W,P) interface. With the increase of aging time, the P elements accumulate to form the continuous P-rich layer. However, the sufficiently high amount of P deteriorates the adherence of IMCs to P-rich layer and consequently leads to the IMC spallation. During the prolonged aging, the Sn elements continuously diffuse across the P-rich layer to react with Co to form the IMCs at the interface neighboring to Co(W,P) while the IMCs neighboring to the molten solder unceasingly spall away. In the meantime, the highly accumulated P elements interrupts the coarsening of IMCs and results in an ultrafine IMC mixture comprising of the P-rich layer [11]. Comprising of reacting interface containing the P-rich layer with fixed thickness in the samples subjected to prolonged aging.

Analytical results regarding to the PbSn/α-Co(W,P) subject to solid-state aging have been reported in detail previously [11]. In conjunction with the results of liquid-state aging presented above, the formation of IMCs apparently implies the sacrificial-type barrier feature of α-Co(W,P) to eutectic PbSn solder. Further, our previous TEM characterization revealed a finely dispersed Co_2P precipitates in the α-Co(W,P) layer and the electroless layer tends to recrystallize during the aging treatment [11]. The formation of phosphide compounds and supersaturated P elements in α-Co(W,P) may block

Fig. 1. Cross-sectional SEM micrographs of PbSn/α-Co(W,P) samples subjected to liquid-state aging at 250 °C for (a) 1 min, (b) 20 min, (c) 30 min, (d) 1 h, (e) 3 h and (f) 5 h.

the diffusion of Cu into Co and, hence, the α-Co(W,P) may also possess the stuffed-type barrier capability since EDS has revealed a negligible interdiffusion between Co and Cu underlayer. The α-Co(W,P) is hence a combined-type, *i.e.*, sacrificial- plus stuffed-type, diffusion barrier.

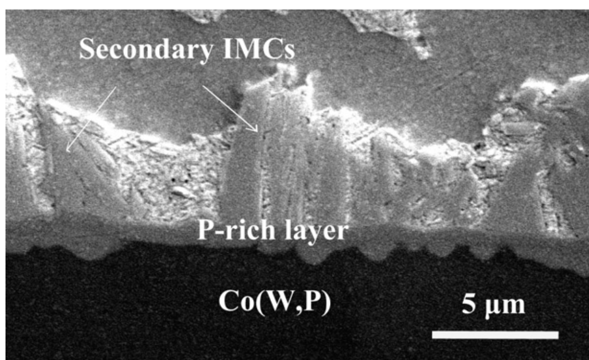

Fig. 2. Cross-sectional SEM micrograph of PbSn/α-Co(W,P) sample subjected to 250 °C/30-min liquid-state aging followed by 150 °C/200-h solid-state aging.

3.2. PbSn/poly-Co(W,P) samples

Fig. 3(a) depicts the cross-sectional SEM image of PbSn/poly-Co(W,P) sample subjected to liquid-state aging for 1 h and the corresponding EDS line scanning profiles is shown in Fig. 3(b). Unlike the sample containing α-Co(W,P), about 5-μm thick, scallop-type $CoSn_3$ IMCs form at the solder/poly-Co(W,P) interface without spallation. In addition, the XTEM/EDS analysis of PbSn/poly-Co(W,P) sample revealed an about 500-nm thick, amorphous layer with relatively high W content ($\sim$15 at.%) emerging in between the $CoSn_3$ IMCs and unreacted Co(W,P) as shown in Fig. 3(c). Since the W content is high in comparison with that in previous α-Co(W,P) system, we hence term it as the W-rich layer. Similar to the accumulation of P, the W-rich layer should result from the accumulation of W at the interface when Co reacts with Sn to form the IMCs due to the low solubility of W elements in the samples.

Since the amorphism has been categorized as a plausible barrier mechanism [1], a liquid-state aging up to 5 h was hence performed to verify whether the W-rich layer may retard subsequent interdiffusion. Nevertheless, the IMC layer was found to thicken to about 7 μm after the 5-h aging in the presence of such an amorphous layer. The decoupling of structure amorphism with

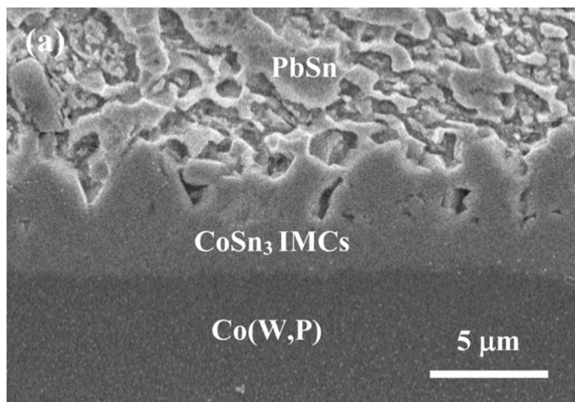

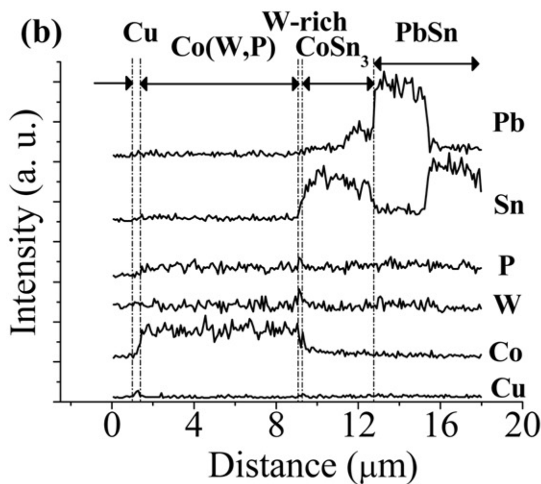

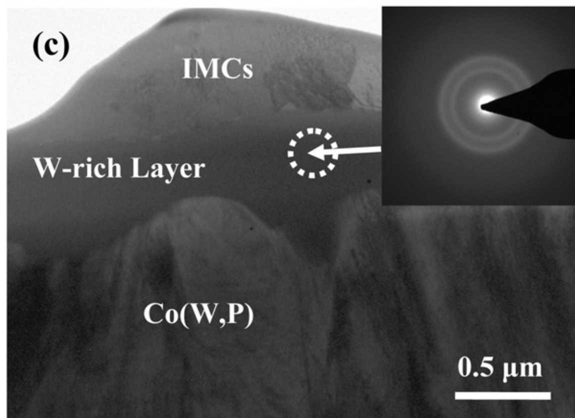

Fig. 3. (a) Cross-sectional SEM micrograph of PbSn/poly-Co(W,P) sample subjected to 250 °C/1-h liquid-state aging and (b) corresponding EDS line scanning profiles. (c) XTEM micrograph of the PbSn/poly-Co(W,P) sample subjected to 250 °C/1-h liquid-state aging. The dotted circle denotes the area where the selected area electron diffraction (SAED) pattern was taken.

the barrier capability was similarly observed in our study regarding of the SnBi/Co(W,P) system [13]. The barrier capability should thus ascribe to the nature of chemical bonds [14], rather than to the structure amorphism as proposed by previous classification scheme [1].

Fig. 4(a) and (b) separately presents the cross-sectional SEM images of PbSn/poly-Co(W,P) samples subjected to solid-state aging for 1000 h and the corresponding EDS line scanning profiles. An about 3 μm in thickness, layer-like IMC formed at the solder/poly-Co(W,P) interface and, according to the EDS analysis, it is mainly the $CoSn_3$ type. The formation of IMCs iterates the sacrificial type barrier feature of poly-Co(W,P) sample.

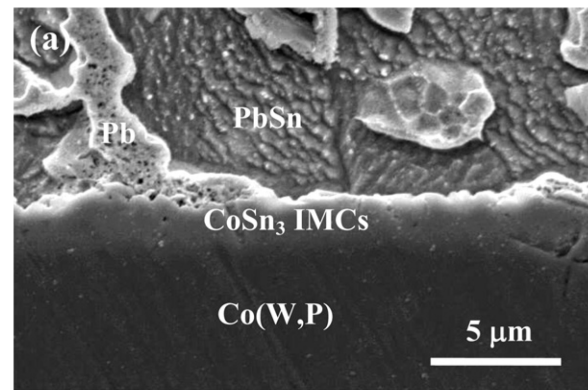

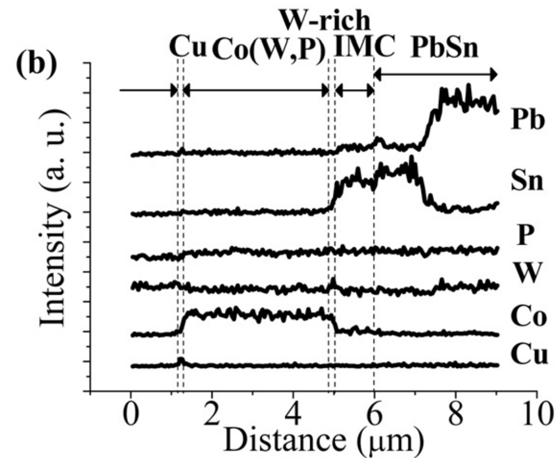

Fig. 4. (a) Cross-sectional SEM micrograph of PbSn/poly-Co(W,P) sample subjected to 150 °C/1000-h solid-state aging and (b) corresponding EDS line scanning profiles.

An XTEM analysis of the 150 °C/1000-h aged sample are presented in Fig. 5. An about 250-nm thick amorphous W-rich layer (W content ∼ 10 at.%) in between IMCs and unreacted Co(W,P) was similarly observed. The thinner W-rich layer in such a sample is attributed to the lower temperature of solid-state aging.

We note that TEM and EDS analyses detect negligible amount of Co_2P precipitates and/or the Co–W alloy phase in unreacted poly-Co(W,P). Although supersaturated P and W contents are present in poly-Co(W,P), their effects on stuffed-type barrier seem comparatively less than those in α-Co(W,P). Besides, the presence of grain boundaries might serve as the fast diffusion paths and subsequent kinetic analysis indicated the poly-Co(W,P) exhibits a lower activation energy of IMC growth. This weakens the stuffed-type barrier capability in poly-Co(W,P) and, hence, the poly-Co(W,P) is mainly as a sacrificial-type barrier.

3.3. Determination of E_a of IMC growth

Fig. 6 presents the thickness consumption of Co(W,P) layer against the square root of aging time in the samples containing various electroless Co(W,P) layers deduced from the SEM characterizations. It can be readily seen that at the same aging time span, less amount of α-Co(W,P) is consumed regardless of the aging type, indicating the α-Co(W,P) possesses a better barrier capability in terms of its sacrificial behavior. It is believed that the barrier capability of α-Co(W,P) layer is enhanced by its high P content which may block the interdiffusion in a more efficient manner in

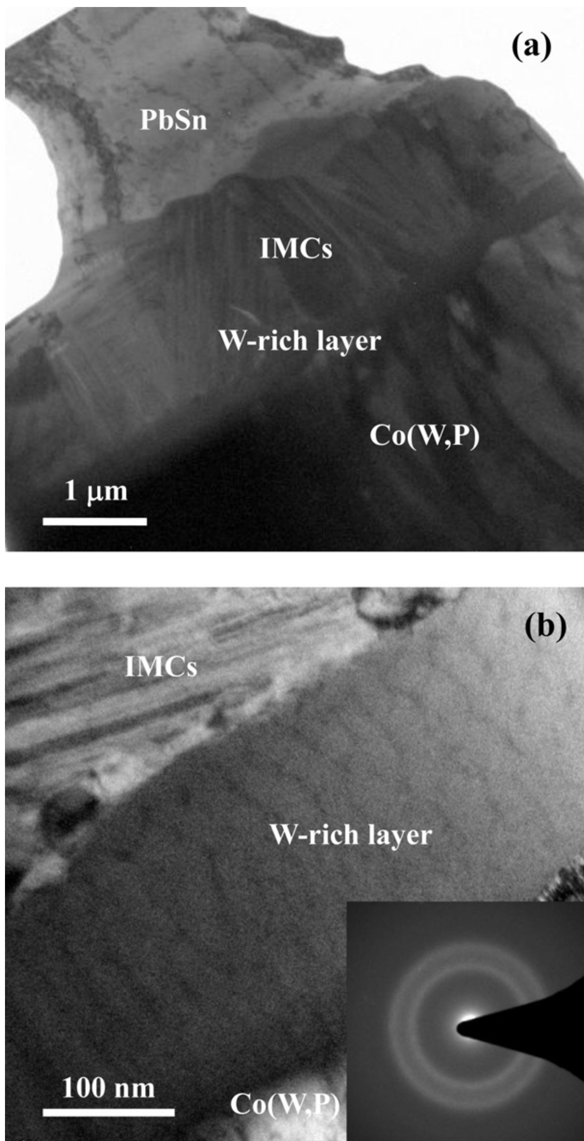

Fig. 5. (a) XTEM micrograph of PbSn/poly-Co(W,P) sample subjected to 150 °C/1000-h solid-state aging. (b) Enlarged picture of W-rich layer and corresponding SAED pattern.

comparison with that in poly-Co(W,P) sample. Fig. 6 also indicates that the consumptions of α-Co(W,P) and poly-Co(W,P) layers subjected to 1-h liquid-state aging are about 1.98 and 2.45 μm, respectively, whereas the consumptions

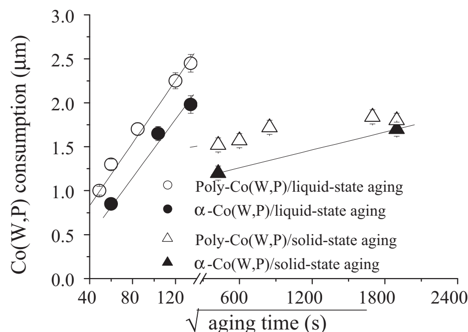

Fig. 6. Consumption of Co(W,P) layer as a function of square root of aging time in the samples containing various electroless Co(W,P) layers.

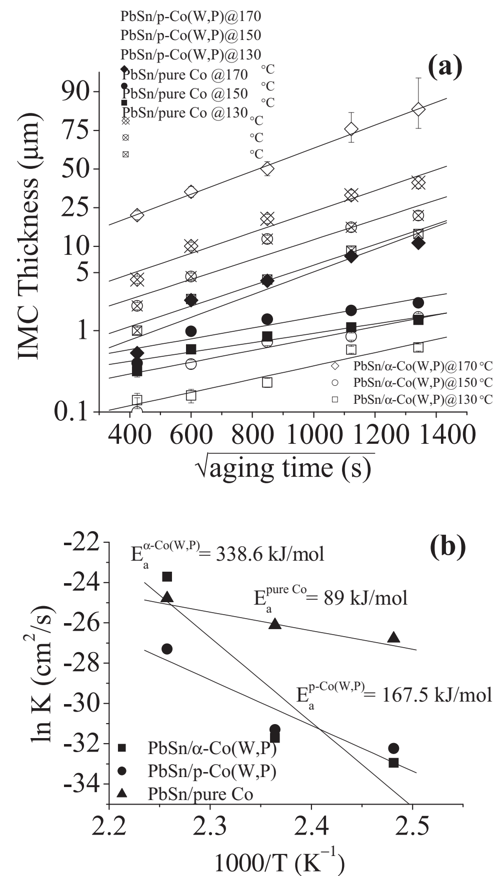

Fig. 7. (a) IMC thickness against the square root of aging time for various PbSn/Co samples subjected to solid-state aging at 130–170 °C up to 500 h. (b) Plots of ln *K* *versus* 1/*T* for the determination of the values of E_a for IMC growth.

of α-Co(W,P) and poly-Co(W,P) layer subjected to 1000-h solid-state aging are about 1.7 and 1.84 μm, respectively. Regardless its crystallinity, an about 2 μm-thick electroless Co(W,P) layer is hence suggested for UBM applied to FC bonding utilizing eutectic PbSn solder joints.

PbSn/α-Co(W,P) and PbSn/poly-Co(W,P) samples subjected to solid-state aging at 130–170 °C up to 500 h were carried out to determine the activation energy (E_a) of IMC growth. For the purpose of comparison, PbSn/pure Co samples were also investigated. As indicated by the plot of IMC thickness as a function of square root of aging time in Fig. 7(a), the linear profiles reveal the diffusion-controlled IMC growth in the time span of investigation. It is well known that the thickness-time relation can be expressed by the formula [15–17]

$$x = \sqrt{Kt} \tag{1}$$

where x = total thickness of IMC layer, t = aging time duration and K = constant correlating to the diffusional growth of IMC. The values of K can be determined from the slopes of plots presented in Fig. 7(a) by employing the Arrhenius form:

$$K = A\,\exp\left(-\frac{E_a}{kT}\right) \tag{2}$$

where A = constant, E_a = activation energy for IMC growth, k = Boltzmann's constant and T = absolute temperature. According to the ln *K* *versus* 1/*T* plot shown in Fig. 7(b), the values of E_a are found to be 338.6, 167.5, and 89 kJ/mol for electroless α-Co(W,P), electroless poly-Co(W,P) and pure Co, respectively. The highest value of E_a for α-Co(W,P) illustrates the best barrier efficiency,

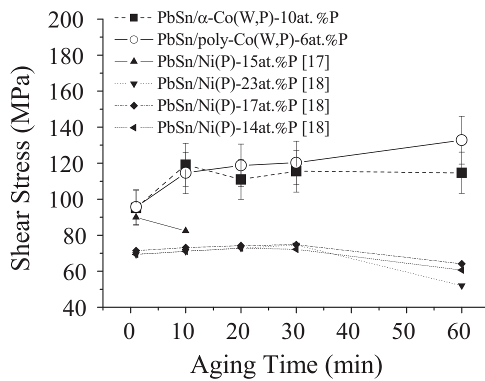

Fig. 8. Shear stresses of PbSn/α-Co(W,P) and PbSn/poly-Co(W,P) samples subjected to liquid-stage aging for various times.

in agreement with the slowest Co thickness consumption and the enhancement of barrier capability due to the high P and W contents in such an electroless layer.

3.4. Shear test

Ball shear tests were carried out to evaluate the mechanical performance of PbSn/Co(W,P) joints subjected to liquid-state aging at various times and the average shear strength is presented in Fig. 8. The test results reported by previous studies regarding of the PbSn/Ni(P) systems [18,19] were also added in Fig. 8 for the purpose of comparison. Fig. 8 indicates the electroless Co(W,P) layers provide a higher bonding strength in comparison with the PbSn/Ni(P) systems. The shear strength of PbSn/α-Co(W,P) sample increases from 95 MPa at as-reflow to a peak value of 119 MPa when aged time is increased to 10 min. The shear strength decreases slightly to 111 MPa in the 20-min aged sample and remains a constant value after 60-min aging. The suppression of bonding strength has been ascribed to the IMC spallation [20,21]. However, according to the failure mode characterization presented below, the decrease of shear strength in PbSn/α-Co(W,P) sample might be correlated to the high P content in electroless layer which suppresses the adhesion strength on Cu underlayer. On the other hand, the PbSn/poly-Co(W,P) sample exhibits a better mechanical performance that the shear strength increases from 95.7 MPa at as-reflow to 132.8 MPa after 1-h aging. Yoon [22] and Sharif [23] also reported the persistence of bonding strength in the Sn–Zn solder/Ni(P) system subjected to 1-h reflow. Such a phenomenon has been ascribed to the sagging of solder due to the weight, resulting in a larger contact area and thus a higher shear force after prolonged reflow [23]. Islam et al. proposed the increment of bonding strength is resulted from the strengthening of solder due to the homogenization during the reflow [24]. Notably, poly-Co(W,P) layer possesses a lower P content in comparison with α-Co(W,P) and there is no IMC spallation in such a system as shown in Fig. 3. The adverse effect due to the P accumulation is expected to be less in PbSn/poly-Co(W,P) system so that a higher interfacial bonding strength is observed.

Failure modes for PbSn/α-Co(W,P) and PbSn/poly-Co(W,P) samples identified in terms of the SEM characterizations and the JESD22-B117A Standard are separately presented in Fig. 9(a) and (b). In as-reflow sample, ductile mode (mode #1), *i.e.*, failure in solder bulk regardless of the existence of dimple failures [12,25], was observed in more than 40% of the 25-tested PbSn/α-Co(W,P) and about 60% of the 25-tested PbSn/poly-Co(W,P) samples. A representative SEM image of ductile failure is shown in Fig. 10(a). Failure at solder/IMC interfaces, *i.e.*, the interfacial break (mode #4), was

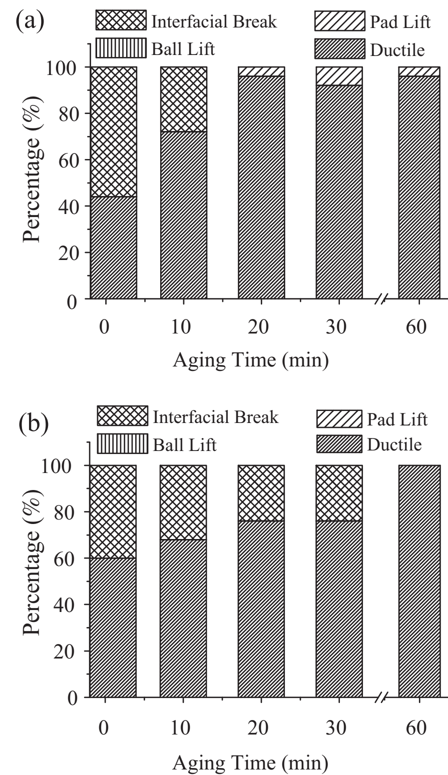

Fig. 9. Summary of failure modes for (a) PbSn/α-Co(W,P) samples and (b) PbSn/poly-Co(W,P) samples.

observed in the rest of as-reflow PbSn/α-Co(W,P) and PbSn/poly-Co(W,P) samples in which the exposure of IMC debris was observed in the fracture surface as shown in Fig. 10(b). The percentage of ductile failure mode increased with the increase of aging time in both samples, indicating a gradual completion of alloy interactions and thus an improvement of bonding strength in between the solder and Co(W,P) layer. Dominance of ductile failure also indicated the interactions of PbSn and Co are fairly strong that it ensures the occurrence of fracture mainly in the bulk of solder. We note the ductile failure in PbSn/α-Co(W,P) samples subjected to prolonged aging is somewhat different from that observed in PbSn/poly-Co(W,P) samples. As shown by a SEM image of PbSn/α-Co(W,P) sample subjected to 20-min aging in Fig. 10(c), relatively flat areas with irregular peripheries was occasionally observed in the fracture surfaces. Solder dewetting might occur on the high-P-content surface and consequently weaken the bonding force of solder bump. The fracture would initiate at the solder/P-rich layer interface and thus cause the exposure of flat P-rich layer surfaces when solder ball is removed. Degradation of solderability due to the accumulation of P elements in EN layer has been reported previously [26] and it might be a cause of bonding strength decrement in PbSn/α-Co(W,P) sample subjected to prolonged aging as shown in Fig. 8. Furthermore, pad lift (mode #2) failure emerged in PbSn/α-Co(W,P) sample aged for more than 20 min. A representative fracture surface morphology is presented in Fig. 10(d). This implies the high P content in α-Co(W,P) might degrade its adherence on Cu underlayer. In addition, the presence of Co_2P precipitate might harden the α-Co(W,P) layer and thus it could not accommodate the thermal stress induced by the glassy transition of Co(W,P) layer which underwent a recrystallization during aging. This caused a breakage of Co(W,P) layer and, hence, the pad lift failure as illustrated in Fig. 10(d).

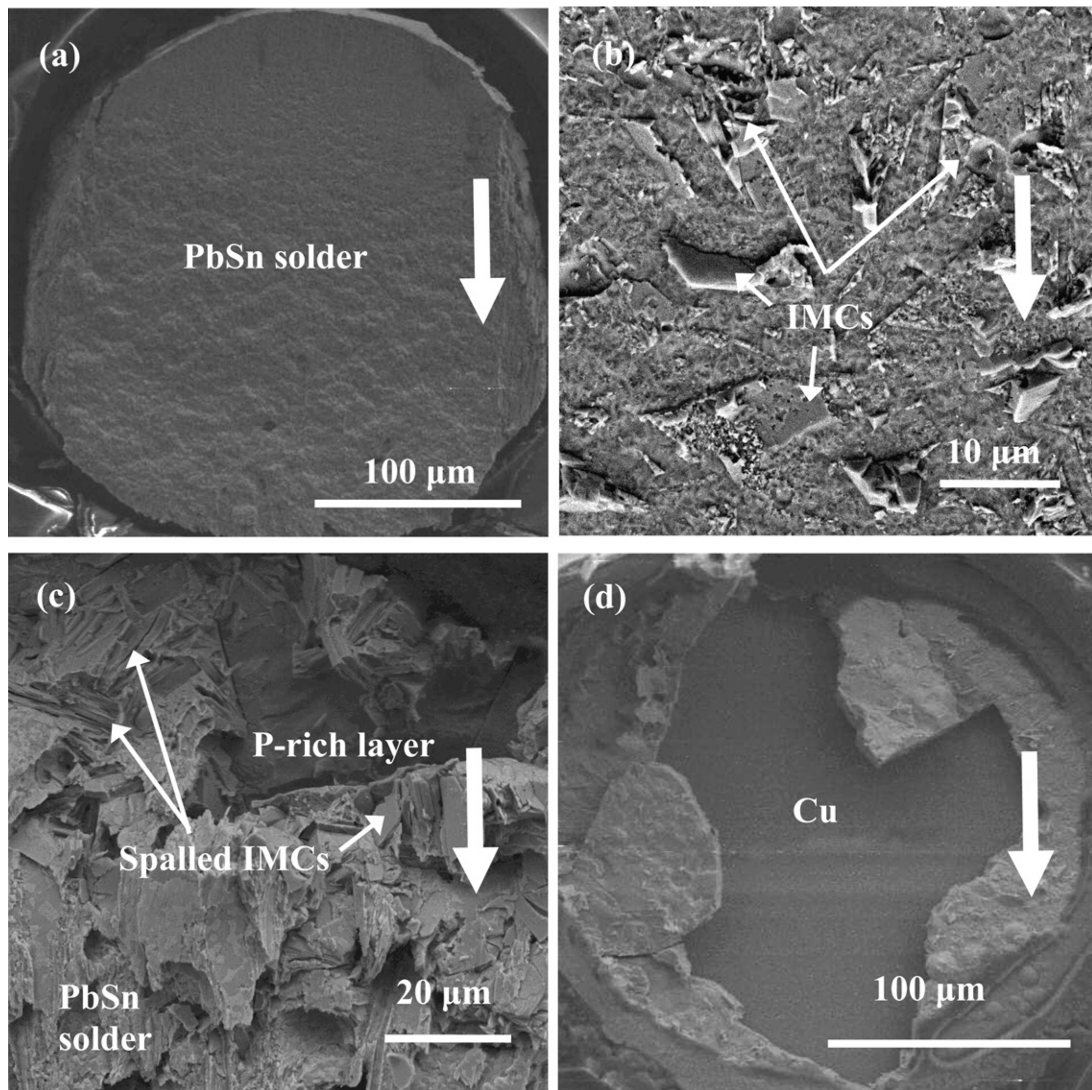

Fig. 10. (a) Ductile failure in as-reflow PbSn/poly-Co(W,P) sample, (b) interfacial break in an as-reflow PbSn/poly-Co(W,P) sample, (c) ductile failure in PbSn/α-Co(W,P) sample subjected to 20-min aging and (d) pad lift in a PbSn/α-Co(W,P) sample subjected to 30-min aging. The arrow in each micrograph indicates the shear direction.

4. Conclusions

In this study, the diffusion barrier characteristics, activation energies of IMC growth and bonding properties of electroless Co(W,P) layers with various crystallinities to PbSn solder are presented. In PbSn/α-Co(W,P) sample subjected to liquid-state aging, spallation of IMCs into solder, formation of polycrystalline P-rich layer and recrystallization of α-Co(W,P) were observed. For the PbSn/α-Co(W,P) subjected to solid-state aging, P-rich layer similarly formed at the interface, however, analytical results indicated such a P-rich layer cannot retard subsequent Co–Sn interactions. The α-Co(W,P) layer was found to serve as a combined type, *i.e.*, the sacrificial- plus stuffed-type, barrier layer. As to PbSn/poly-Co(W,P) samples, the $CoSn_3$ IMCs neighboring to an amorphous W-rich layer was observed at the solder/Co(W,P) interface regardless of aging types. The poly-Co(W,P) layer served mainly as a sacrificial-type barrier. Similar to the P-rich layer, the amorphism of W-rich layer did not provide the barrier capability in the samples.

The activation energies of IMC growth in PbSn/α-Co(W,P), PbSn/poly-Co(W,P) and PbSn/pure Co samples deduced from the solid-state aging were found to be 338.6, 167.5 and 89 kJ/mol, respectively. This illustrated the presence of P and W elements in electroless layers may enhance the diffusion barrier capability.

Shear test revealed a dominance of ductile failure in both PbSn/α-Co(W,P) and PbSn/poly-Co(W,P) samples, indicating a promising application of such electroless layers as the diffusion barriers in UBM structure. However, relatively high P content in α-Co(W,P) might be a concern on the applications since it caused adverse effects on the solderability and would degrade the mechanical performance of FC bonding.

Acknowledgments

This work was supported by the National Science Council of Republic of China under Contract No. NSC 95-2221-E-009-130. SEM/TEM/EDS analyses and the FIB technique for preparation of XTEM specimens supported by Materials Analysis Technology, Inc., Chupei, Taiwan, ROC, and shear test apparatus supported by Schmidt Scientific Taiwan Ltd. at Hsinchu, Taiwan, ROC, are also acknowledged.

References

[1] M.A. Nicolet, Thin Solid Films 52 (1978) 415–443.
[2] R.H. Uang, K.C. Chen, S.W. Lu, H.T. Hu, S.H. Huang, IEEE Electron. Pack. Technol. Conf. (2000) 292.

[3] M.W. Liang, T.E. Hsieh, C.C. Chen, Y.T. Hung, Jpn. J. Appl. Phys. 43 (2004) 8258–8266.
[4] T. Oppert, E. Zakel, T. Teutsch, Proc. IEMT/IMC Symp. (1998) 106.
[5] T. Teutsch, T. Oppert, E. Zakel, E. Klusmann, Electron. Comp. Technol. Conf. (2000) 107.
[6] G.O. Mallory, J.B. Hajdu, Electroless Plating Fundamentals and Applications, AESF, Orlando, Florida, 1990 (Chap. 1–7).
[7] E.J. O'Sullivan, A.G. Schott, M. Paunovic, C.J. Sambucetti, J.R. Marino, P.J. Bailey, S. Kaja, K.W. Semkow, IBM J. Res. Dev. 42 (1998) 607–620.
[8] M.W. Liang, H.T. Yen, T.E. Hsieh, J. Electron. Mater. 35 (2006) 1593–1599.
[9] A. Kohn, M. Eizenberg, Y. Shacham-Diamand, Y. Sverdlov, Mater. Sci. Eng. A 302 (2001) 18–25.
[10] A. Kohn, M. Eizenberg, Y. Shacham-Diamand, B. Israel, Y. Sverdlov, Microelectron. Eng. 55 (2001) 297–303.
[11] W.C. Wu, T.E. Hsieh, H.C. Pan, J. Electrochem. Soc. 155 (2008) D369–D376.
[12] JEDEC Standard, JESD22-B117A.
[13] H.C. Pan, T.E. Hsieh, J. Electron. Mater. 40 (2011) 330–339.
[14] D.A. Porter, K.E. Easterling, Phase Transformations in Metals and Alloys, Chapman & Hall, London, 1981 (Chap. 1).
[15] V.I. Dybkov, O.V. Duchenko, J. Alloys Compd. 234 (1996) 295–300.
[16] A. Sharif, Y.C. Chen, Mater. Sci. Eng. B 106 (2004) 126–131.
[17] D.Q. Yu, C.M.L. Wu, C.M.T. Law, L. Wang, J.K.L. Lai, J. Alloys Compd. 392 (2005) 192–199.
[18] D.G. Kim, J.W. Kim, S.S. Ha, B.I. Noh, J.M. Koo, D.W. Park, M.W. Ko, S.B. Jung, J. Alloys Compd. 458 (2008) 253–260.
[19] M.O. Alam, Y.C. Chan, K.C. Hung, Microelectron. Reliab. 42 (2002) 1065–1073.
[20] C.B. Lee, S.B. Jung, Y.E. Shin, C.C. Shur, Mater. Trans. 43 (2002) 1858–1863.
[21] P.C. Shih, K.L. Lin, J. Alloys Compd. 422 (2006) 153–163.
[22] J.W. Yoon, H.S. Chun, S.B. Jung, Mater. Trans. 46 (2005) 2386–2393.
[23] A. Sharif, Y.C. Chan, J. Alloys Compd. 440 (2007) 117–121.
[24] M.N. Islam, Y.C. Chan, A. Sharif, M.O. Alam, Microelectron. Reliab. 43 (2003) 2031–2037.
[25] S.M.L. Nai, J. Wei, M. Gupta, J. Alloys Compd. 473 (2009) 100–106.
[26] J.J. Guo, A.P. Xian, J.K. Shang, Surf. Coat. Technol. 202 (2007) 268–274.